Physics of the Earth and Planetary Interiors 299 (2020) 106412

Contents lists available at ScienceDirect

Physics of the Earth and Planetary Interiors

journal homepage: www.elsevier.com/locate/pepi

Possible H_2O storage in the crystal structure of $CaSiO_3$ perovskite

H. Chen[a], K. Leinenweber[b], V. Prakapenka[c], C. Prescher[c,d], Y. Meng[e], H. Bechtel[f], M. Kunz[f], S.-H. Shim[a,*]

[a] School of Earth and Space Exploration, Arizona State University, Tempe, AZ, United States of America
[b] Eyring Materials Center, Arizona State University, Tempe, AZ, United States of America
[c] Center for Advanced Radiation Sources, University of Chicago, Chicago, IL, United States of America
[d] Deutsches Elektronen-Synchrotron, Hamburg, Germany
[e] HPCAT, Advanced Photon Source, Argonne National Laboratory, IL, United States of America
[f] Advanced Light Source, Lawrence Berkeley National Laboratory, Berkeley, CA, United States of America

ARTICLE INFO

Keywords:
$CaSiO_3$ perovskite
Water
Mantle

2010 MSC:
00-01
99-00

ABSTRACT

The lower mantle is believed to contain much less hydrogen (or H_2O) because of the low storage capacity of the dominant mineral phases, such as bridgmanite and ferropericlase. However, possible hydrogen storage in the third most abundant mineral in the region, $CaSiO_3$ perovskite (Ca-Pv), is not well unknown. We have synthesized Ca-Pv from different starting materials with varying H_2O contents at 19–120 GPa and 1400–2200 K in laser-heated diamond-anvil cell. While cubic perovskite structure is stable at the mantle-related pressures-temperatures ($P-T$) in anhydrous systems, we found non-cubic diffraction peak splitting in Ca-Pv even at high temperatures when it is synthesized from hydrous starting materials. In-situ high-pressure infrared spectroscopy showed OH vibration possibly from Ca-Pv. The unit-cell volume of hydrothermally synthesized Ca-Pv is systematically smaller than that of anhydrous Ca-Pv at high pressures. These observations suggest possible H_2O storage in Ca-Pv at mantle-related $P-T$ conditions. We also found the formation of separate δ–AlOOH and Ca-Pv phases from Al-bearing $CaSiO_3$ glass starting materials in an H_2O medium at 60 GPa and 1400 K. Ca-Pv still showed non-cubic peak splitting at high temperatures in this experiment. Therefore, it is possible that hydrous phases may coexist together with hydrous Ca-Pv in the lower mantle.

1. Introduction

The capabilities of mantle silicate minerals to store OH are the keys to understand the possible existence and concentration of hydrogen in the deep mantle. High-pressure experiments have shown that some nominally anhydrous minerals (NAMs) can store significant amounts of hydrogen in the mantle. For example, olivine and garnet in the upper mantle can store ~200 ppm H_2O (Smyth et al., 2006), while wadsleyite and ringwoodite in the mantle transition zone can contain up to 3 wt. % H_2O (Inoue et al., 1995; Ye et al., 2010). The amount of hydrogen in the lower mantle has not been well constrained, despite the fact that the lower mantle represents about 55% of the Earth's volume. The most dominant mineral, bridgmanite, seems to store less than 200 ppm H_2O (Bolfan-Casanova et al., 2000), and ferropericlase can contain no more than 20 ppm water (Bolfan-Casanova et al., 2003). These results lead to a view that the lower mantle is much more dry than the layers above (Bolfan-Casanova et al., 2003; Panero et al., 2015).

However, $CaSiO_3$ perovskite (Ca-Pv), the third most abundant phase in the lower mantle (Kesson et al., 1998), has not been well studied for possible H_2O storage. Murakami et al. (2002) reported 0.4 wt. % H_2O in Ca-Pv synthesized from a pyrolitic multi-component system under H_2O saturated conditions. However, later reports have suggested possible existence of hydrous phases in the samples synthesized under similar conditions and therefore possible contamination of OH signal from those hydrous mineral phases (Bolfan-Casanova, 2005). Recently from textural and compositional observations based on quenched samples, Németh et al. (2017) inferred possible solubility of H_2O in Ca-Pv. However, they could not find any evidence for OH mode in their infrared spectra (IR) of the recovered samples.

Ca-Pv has been consistently shown to be unstable at 1 bar and convert to glass (Wang et al., 1996; Shim et al., 2000b; Chen et al., 2018). This property makes the high-precision characterization and quantification of H_2O very difficult for Ca-Pv, because such techniques, for example Thermo-Gravimetric Analysis (TGA) and Secondary Ion Mass Spectrometry (SIMS), are normally not applicable for the samples in a high-pressure apparatus. In situ high-pressure measurements are

* Corresponding author.
E-mail address: shdshim@gmail.com (S.-H. Shim).

https://doi.org/10.1016/j.pepi.2019.106412
Received 16 August 2019; Received in revised form 26 November 2019; Accepted 20 December 2019
Available online 23 December 2019
0031-9201/

possible in IR spectroscopy. However, the technique has not been applied for estimation of H_2O in the samples under high pressure as much, because of larger uncertainties, such as background signal from diamond anvils.

Another important hydrogen storage to consider in addition to NAMs (such as bridgmanite, ferropericlase, and Ca-Pv) is a series of hydrous phases found in recent experiments (see reviews in Ohtani, 2015), such as phase egg (Eggleton and Ringwood, 1978), δ–AlOOH (Sano et al., 2008), phase D (Frost and Fei, 1998), phase H (Nishi et al., 2014) and FeOOH (Gleason et al., 2013; Liu et al., 2017; Nishi et al., 2017). Although their high-temperature stability is still under investigation (Sano et al., 2008; Nishi et al., 2014; Duan et al., 2018), it is uncertain if they can be stabilized in the presence of NAMs and if lower-mantle NAMs can contain hydrogen.

In order to understand possible storage of hydrogen in Ca-Pv in a form of OH, we have conducted high-pressure synthesis of Ca-Pv with a range of starting materials with varying amount of H_2O. Although the exact quantification of H_2O stored in Ca-Pv remains challenging, we found a line of evidence which can support possible H_2O storage in Ca-Pv.

2. Experimental methods

We have prepared three different materials as starting materials of the laser-heated diamond-anvil cell (LHDAC) experiments. We synthesized $CaSiO_3$ glass using the laser levitation method (Tangeman et al., 2001). Xonotlite was synthesized from CaO, SiO_2 (Alfa-Aesar), and water at 1 GPa and 500 °C using a piston cylinder apparatus at the Depth of the Earth lab of Arizona State University (ASU) (Shaw et al., 2000). We confirmed the composition of the synthetic xonotlite to be pure $CaSiO_3$ in 2010F (JEOL) electron microprobe. We used natural sample for suolunite from Quebec, Canada. The crystal structures and purity of the suolunite and xonotlite samples were also examined with synchrotron X-ray diffraction at 13IDD beamline of the GeoSoilEnviroConsortium for Advanced Radiation Sources (GSECARS) sector at the Advanced Photon Source (APS). Xonotlite, $Ca_6Si_6O_{17}(OH)_2$, contains 2.5 wt. % H_2O, and suolunite, $Ca_2(H_2Si_2O_7)\cdot H_2O$, contains more than 13 wt. % H_2O (Ma et al., 1999; Shaw et al., 2000). The diffraction patterns are in good agreement with the reported diffraction patterns of these minerals (Ma et al., 1999; Shaw et al., 2000).

These three different starting materials were separately powdered. Each of them is mixed with 10 wt. % Pt for the internal pressure standard (Ye et al., 2017) and laser coupling. The powder mixtures are then cold-compressed to thin foils. A thin foil was loaded into the sample chamber made in a Re gasket. Several spacers less than 10 μm from pure samples were placed below and above the sample foil to form a layer of Ne or Ar (for xonotlite and suolunite starting materials) or H_2O (for glass + water mixture) between sample and diamond anvils for thermal insulation. Neon was loaded as a pressure medium in the the gas-loading system at GSECARS (Rivers et al., 2008). Argon was cryogenically loaded at ASU. The experimental runs we made are listed in Table 1. They all produced pure Ca-Pv except for run al211 where we observed Ca-Pv and δ-AlOOH.

We measured X-ray diffraction (XRD) patterns in the LHDAC at beamline 13ID-D in the GSECARS sector (Prakapenka et al., 2008) and beamline 16ID-B in the High Pressure Collaborative Access Team (HPCAT) sector (Meng et al., 2006) at the APS. The focus sizes of the monochromatic X-ray beams were 3×4 and 5×6 μm^2 at GSECARS and HPCAT, respectively, at the samples. Diffraction patterns were collected using a Mar-CCD detector.

Two near-infrared laser beams (~1 μm wavelength) were focused on both sides of the sample through two opposite sides of DAC with a hot spot size- > diameter of 20–25 μm at synchrotron beamlines. The laser beams were aligned coaxially with the X-ray beam before laser heating. We used X-ray wavelength of 0.4959 or 0.4066 Å. Temperatures were calculated by fitting the thermal radiation spectra from both sides of the sample to the Planck equation after subtracting backgrounds.

Table 1
Conditions of the high-pressure experimental runs. SM: starting materials, Suo: Suolunite, Xon: Xonotlite, Gla: $CaSiO_3$ glass, Al-Gla: $0.95CaSiO_3\cdot0.05Al_2O_3$ glass, Tet: Tetragonal, Cub: Cubic, Medium: Pressure Medium, *P*: Pressure, *T*: Temperature, *: CO_2 heating for IR spectroscopy measurements, Str: crystal structure.

Run	SM	Product	Str.	Medium	*P* (GPa)	*T* (K)
x231	Xon	Ca-Pv	Cub	Ne	115	2000–2600
x310	Xon	Ca-Pv	Cub	Ne	31	1300–1700
s320	Suo	Ca-Pv	Tet	Water	30	1700
s111*	Suo	Ca-Pv	Tet	Ar	19	1400
s110	Suo	Ca-Pv	Tet	Ne	60	1300–2100
s431	Suo	Ca-Pv	Tet	Ne	45	1500–2200
s332	Suo	Ca-Pv	Tet	Ne	120	2300
s411	Suo	Ca-Pv	Tet	Ne	60	2000–2300
g211	Gla	Ca-Pv	Tet	Water	30	1400
g320	Gla	Ca-Pv	Tet	Water	60	1400–1600
al211	Al-Gla	Ca-Pv + AlOOH	Tet	Water	60	1400

In a typical experiment, we compressed the sample to target pressures at 300 K, and then conducted laser heating. Xonotlite and suolunite amorphize below 40 GPa during cold compression to target pressures. We increased the laser power quickly to reach the target temperatures between 1400 and 2300 K in less than 1 min to avoid the formation of possible metastable structures. Ca-Pv formed within 1 min upon heating above 1400 K and diffraction patterns of Ca-Pv remained essentially the same with further heating. After heating, room-temperature diffraction patterns were also acquired on the heated spot at each target pressure. We also measured diffraction patterns at different spots around the heating spots.

We integrated 2D diffraction images in the Dioptas package (Prescher and Prakapenka, 2015). We performed phase identification and peak fitting using a pseudo-Voigt profile shape function in PeakPo (Shim, 2017). The data obtained from the GSECARS and HPCAT beamlines agreed well with each other.

A separate CO_2 heating experiment was conducted to prepare Ca-Pv samples for infrared spectroscopy measurements using a heating system at ASU. For the CO_2 heating, we did not load any laser coupler because silicates can couple directly with CO_2 laser. For this experiment, Ar was cryogenically loaded as a medium in a DAC. A ruby chip was loaded at the edge of the sample chamber for pressure measurements but away from the sample foil in order to avoid any chemical reaction. We compressed the samples with type-II diamond anvils and focused a CO_2 laser beam on the sample foil in the DAC. Single-sided heating was conducted at 1400 K. The diameter of the laser heating spot was ~50 μm. Temperatures were calculated by fitting the measured thermal radiation spectra to the Planck equation from one side of the sample after the subtracting backgrounds from optics in the system. Pressure was measured from ruby fluorescence line shift or the first-order Raman mode from the tips of the diamond anvils (Mao et al., 1978; Akahama and Kawamura, 2006).

The sample we synthesized using CO_2 laser heating was then transported to the beamline 1.4 of the Advanced Light Source (ALS) for IR measurements. The sample was in DAC and still under high pressure. We used a Nicolet Magna 760 FTIR spectrometer with a custom microscope and a HgCdTe detector. The spectral resolution of the system is 4 cm^{-1}. The spectra were measured over 256 scans.

For the analysis of the IR spectra, we fit the OH band with pseudo-Voigt profile shape function in the LMFIT package (Newville et al., 2015) for the positions and the widths. We estimated the content of H_2O from the IR spectra using the Paterson's method (Paterson, 1982):

$$C_{H_2O} = \frac{X_i}{150\zeta}\int \frac{k(v)}{3780 - v}dv, \quad (1)$$

where C_{H_2O} is H_2O content in ppm and X_i is the density factor for Ca-Pv, which we used 2127. $X_i = 10^6 \times (18/2d)$, where d is the mineral density in g/l. We used a value of 4.23 g/cm^3 for the density of Ca-Pv based on extrapolated unit-cell volume at 1 bar (Shim et al., 2002). Although we obtain relatively accurate thickness at 1 bar (12 μm), the thickness is the major uncertainty source at high pressure (we discuss this later). Combined with the limited pressure range for the IR measurements (0–19 GPa), the assumed density above does not contribute to the estimation of H_2O content as much. ζ is the crystal orientation factor and in this case we used 1/3, assuming that the Ca-Pv crystals are randomly oriented in the DAC. $k(\nu)$ is absorption coefficient for infrared band in cm^{-1}. ν is the wavenumber of the OH band.

3. Result and discussion

Previous experimental and theoretical studies have found that Ca-Pv has a tetragonal perovskite structure at low temperatures and high pressures (Stixrude et al., 1996; Shim et al., 2002; Kurashina et al., 2004). However, Ca-Pv undergoes a phase transition from tetragonal to cubic at ~500 K and the cubic structure is stable at higher temperatures relevant to those expected for the mantle (Kurashina et al., 2004; Chen et al., 2018). In our experiments on the xonotlite starting material with 2.5 wt. % H_2O, Ca-Pv showed a relatively sharp 200_{pc} peak (subscript "pc" means Miller index of a pseudo-cubic unit cell) in the unrolled diffraction images (Fig. 1a). Upon temperature quench at high pressures, the peak broadens severely, consistent with the peak splitting effect expected for the cubic to tetragonal transition (Kurashina et al., 2004; Chen et al., 2018).

In the experiments with the suolunite starting materials with a larger H_2O content (13 wt. %), Ca-Pv showed clear peak splitting of the 200_{pc} line even at 1800 K in a Ne pressure transmitting medium (Fig. 1b and d). Because of the limited resolution, it is difficult to conclusively assign to tetragonal distortion and rule out the possibility of a lower symmetry structure. However, the diffraction spots can be largely aligned to two diffraction features in the figure and therefore we tentatively assign tetragonal for the distorted structure observed for Ca-Pv. Upon temperature quench at high pressure, the peak splitting remains in the diffraction patterns.

We further increased the amount of H_2O in the sample chamber by loading water as a medium. Although the temperatures we can reach were lower than those we achieved for the suolunite runs likely because of the H_2O melting, the peak splitting was also found in this H_2O saturated experiments as shown in Fig. 1c. The diffraction spots are more clearly aligned to two diffraction lines, supporting our assignments of the structure to a tetragonal structure. H_2O in solid state may develop deviatoric stress when it is used as a medium (Wolanin et al., 1997). However, we note that the splitting was observed at temperatures very close or even higher than the melting of H_2O ice (Lin et al., 2004; Schwegler et al., 2008). Therefore, it is unlikely that the deviatoric stress plays a role for the observation of the peak splitting at high temperature. We also note that the high-temperature peak splitting of Ca-Pv was also found in a Ne medium in our suolunite experiments.

The importance of this observation is that tetragonal Ca-Pv remains stable even at temperatures much higher than 500 K previously reported for the phase transition to cubic structure (Kurashina et al., 2004). In fact, the stability of tetragonal structure was observed at temperatures related to the subducting slabs and even the normal mantle in our experiments when H_2O is present in the system (Table 1).

Because the only difference from previous experiments of cubic Ca-Pv (Kurashina et al., 2004; Chen et al., 2018) is the presence of H_2O, we interpret that the different structural behavior of Ca-Pv at high temperature, i.e., stability of non-cubic distorted perovskite structure, as a sign of H_2O incorporation in the crystal structure of Ca-Pv. The reason that Ca-Pv synthesized from xonotlite (with the lowest H_2O content

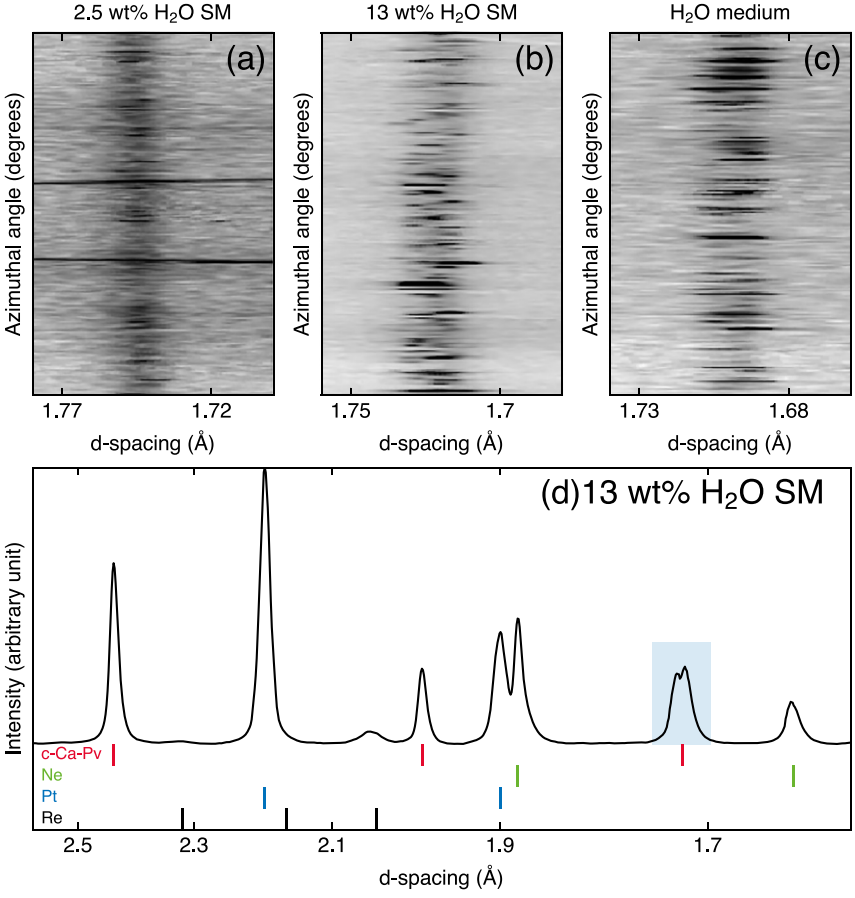

Fig. 1. In-situ X-ray diffraction data of Ca-Pv synthesized from hydrous starting materials at high pressure and high temperature. Unrolled diffraction images for the 200_{pc} line of Ca-Pv synthesized from (a) xonotlite (2.5 wt.% H_2O) at 30 GPa and 2000 K, (b) suolunite (13 wt.% H_2O) at 40 GPa and 1800 K, and (c) $CaSiO_3$ glass + H_2O (H_2O saturated condition) at 48 GPa and 1400 K. We observed clear peak splitting for the 200_{pc} line of Ca-Pv with H_2O rich starting materials. An integrated 1D diffraction pattern of (b) is shown in (d) for a wider 2θ angle range. The cyan highlighted area in (d) is shown in (b). In (d), the vertical ticks are the calculated peak positions expected for cubic Ca-Pv (c-Ca-Pv), platinum (Pt; laser coupler), neon (Ne; pressure medium), and rhenium (Re; gasket material). We also provided the H_2O contents of the starting materials (SM) used for the synthesis.

among our starting materials) does not show detectable distortion could be: there was not enough amount of H_2O incorporated into Ca-Pv, so that little to no distortion was made for the crystal structure at high temperatures. It is also possible that the distortion exists even for Ca-Pv synthesized from xonotlite but it results in only subtle splitting below the detection level of the diffraction setup we used. In Fig. 1a, peak splitting can be inferred from a few dots in the unrolled diffraction image but it is difficult to conclude the existence of the distortion in the case of the xonotlite runs. However, Fig. 1a–c shows that the peak splitting becomes clearer with an increase in the amount of H_2O in the starting material.

Infrared (IR) spectroscopy is sensitive to the trace amount of OH incorporated into the structure of materials and method has been developed for estimating the amount of H_2O exists in the materials, such as Paterson's method (Paterson, 1982). For IR measurements, we performed CO_2 laser heating on the suolunite starting material in an Ar medium at 19 GPa and 1400 K. The X-ray diffraction patterns from the sample shows successful conversion of the starting material to Ca-Pv at beamline 12.2.2. of the Advanced Light Source. Because CO_2 laser couples directly with silicates, we did not include platinum metal for laser coupling, which enhances the quality of the measured IR spectra. After laser heating and XRD measurements, we conducted IR measurements at in situ high pressure. We found an intense broad band at a wavenumber range of 3100–3600 cm^{-1} from the heated area as shown in Fig. 2a. The band position shifts to a lower frequency with an increase in pressure (Fig. 2b). The peak position is different from that of the OH mode in H_2O ice (Goncharov et al., 1996) at pressures above 5 GPa. Therefore, the mode is likely from Ca-Pv, suggesting possible incorporation of OH in the crystal structure of Ca-Pv. Because we do not know the exact amount of H_2O in Ca-Pv (although we estimated below), it is difficult to rule out the possibility of some contribution of H_2O released from the starting material to the observed IR intensity. This might explain the broadness of the OH band we found in this study. However, the distinct wavenumber position of the observed OH modes suggests more contributions of OH vibration other than H_2O ice, possibly from Ca-Pv.

The negative shift of the OH phonon frequency has been observed in high pressure ice and was attributed to the symmetrization of the O—H bond (Goncharov et al., 1996). The symmetric O—H bonding would have a centered hydrogen in between two oxygen atoms. Therefore, the possible transition from (more) symmetric to asymmetric H—O—H could be responsible for the increase in wavenumber of the OH mode (therefore strengthening O—H bonding) during decompression we observed for the Ca-Pv sample.

It is notable that the OH mode frequency becomes similar to that of the OH mode from H_2O near 1 bar (Fig. 2). Ca-Pv transforms into a glass state at about 1 GPa (Wang et al., 1996). It is possible that the storage capacity of $CaSiO_3$ glass may be smaller than that of Ca-Pv and therefore H_2O could be released during amorphization at pressures lower than 1 GPa. However, at 1 bar we have very little intensity in the OH region of the IR spectra (Fig. 2). The observation suggests that the H_2O possibly released from the sample may be evaporated as we opened the diamond-anvil cell for the recovery measurements. We attempted to calculate the H_2O content of Ca-Pv from the high-pressure IR using the Paterson method (Paterson, 1982). The absorbance was obtained after subtracting the background spectra which was measured for the Ar-only spots in the DAC sample chamber.

We obtained an H_2O content of 0.5–1 wt. %. The Paterson's method has been mostly applied to IR spectra measured at room temperature and pressure (Bolfan-Casanova, 2005). We found that the application of the method to high pressure data measured in LHDAC is challenging. The most notable uncertainty comes from the thickness of the sample. The thickness of the sample foil was approximately 20 μm before compression and was approximately 12 μm after pressure quench. Therefore, our estimation assumed a thickness of 10–20 μm for the sample at high pressures. A smaller thickness might overestimate the H_2O content from the Paterson's equation (Paterson, 1982).

Another possible uncertainty source in our measurements is H_2O released from the starting material during the laser heating if not all H_2O is incorporated into the crystal structure of Ca-Pv. When H_2O is released as a liquid phase, it can disperse into the pressure medium and also grain boundaries of Ca-Pv. Fraction of H_2O dispersed outside of the heating spot to the medium or grain boundaries outside of the heated area would not contribute to the IR intensity we measured. However, the fraction of H_2O remained along the path of our IR beam would contribute to the IR intensity of the observed OH band. From this possibility, our estimation can be regarded as upper bound for the H_2O storage capacity of Ca-Pv.

Some degree of dissolution of the $CaAlO_{2.5}$ component in Ca-Pv has been found in previous high pressure experiments (Bläß et al., 2007). Furthermore, incorporation of H_2O through $Al^{3+} + H^{+} \rightarrow Si^{4+}$ has been considered for mantle silicates (Pawley et al., 1993; Navrotsky, 1999; Litasov et al., 2003, 2007). Therefore, we also conducted experiments on aluminum bearing $CaSiO_3$ glass ($0.95CaSiO_3 \cdot 0.05Al_2O_3$) in an H_2O medium. With laser heating to 1700 K at 47 GPa (Fig. 3), Ca-Pv peaks appeared immediately. Similar to the case of the experiments with the suolunite and glass + H_2O starting materials, we found the splitting of the 200_{pc} peak at high temperatures (inset of Fig. 3a). In this experiment, a few weak but clear extra lines appeared within 10 min of laser heating. They can be well indexed as the lines of δ-AlOOH as demonstrated in Fig. 3a.

In the diffraction patterns we measured for the recovered samples of

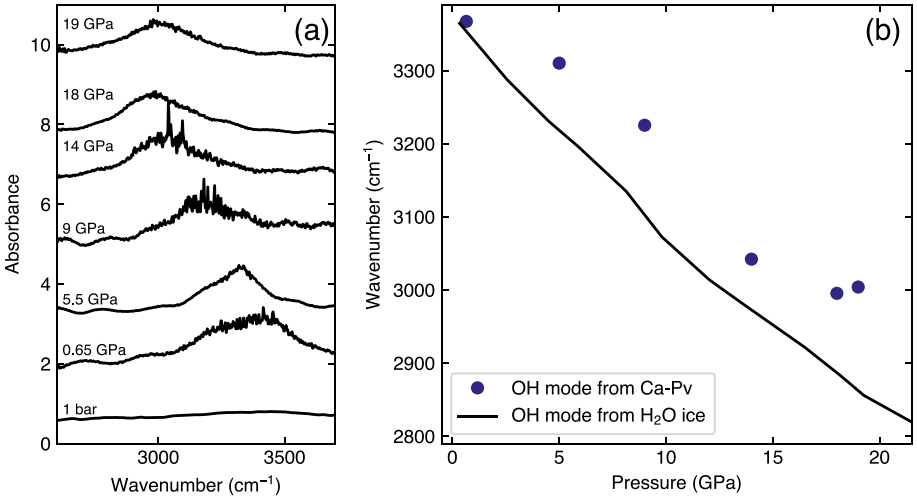

Fig. 2. (a) Infrared spectra of the OH band from the Ca-Pv samples synthesized from the suolunite staring material in an Ar medium at 19 GPa and 1700 K. We measured IR spectra at different pressures during decompression. (b) We compare the observed wavenumber of the OH band from the Ca-Pv sample with the IR active OH band from H_2O ice reported in Goncharov et al. (1996).

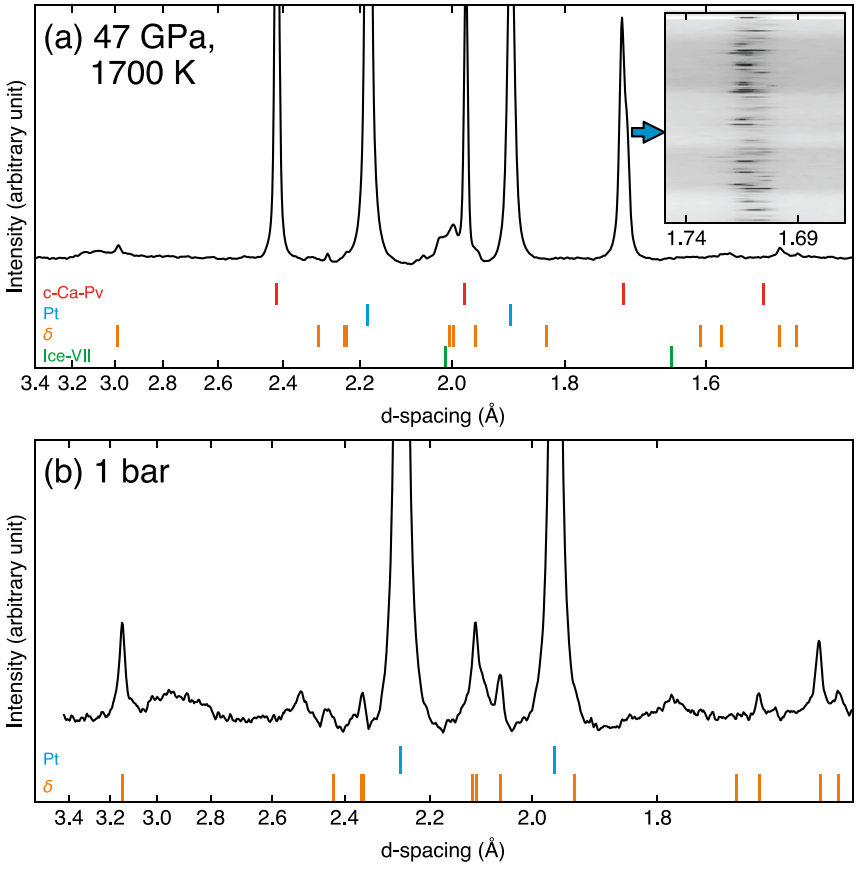

Fig. 3. (a) In-situ X-ray diffraction patterns of Ca-Pv and δ-AlOOH formed from the $0.95CaSiO_3{\cdot}0.05Al_2O_3$ + H_2O starting mixture at 47 GPa and 1700 K. The inset in (a) shows the clear peak splitting of the 200_{pc} line of Ca-Pv. We also present diffraction pattern from the quenched sample of the experimental run in (b). The vertical ticks are the calculated peak positions expected for cubic Ca-Pv (c-Ca-Pv), δ-AlOOH (δ), platinum (Pt; laser coupler), and H_2O ice-VII (Ice-VII; medium). The unit-cell volume for δ–AlOOH is 56.4(1) $Å^3$ at 1 bar, which is in good agreement with the reported value, 55.97 $Å^3$ (Kudoh et al., 2004), considering the quality of diffraction patterns we obtained from a very small amount of δ-AlOOH. The wavelength of the X-ray beam is 0.4066 Å.

the run, the diffraction peaks of δ-AlOOH remain visible. In contrast, we found no diffraction peaks from Ca-Pv. δ-AlOOH is known to be quenchable to 1 bar (Suzuki et al., 2000), while Ca-Pv is known to transform to glass with decompression (Wang et al., 1996; Shim et al., 2000b).

Ca-Pv is known to accommodate Al into the crystal structure up to 10 wt. % (Gréaux et al., 2011). However, Al forms a separate hydrous phase under H_2O saturated conditions in our experiments. It is also important to point out that Ca-Pv may contain H_2O at the same time, inferred from the peak splitting at high temperatures. This observation indicates that the existence of H_2O can change the partitioning behavior of Al in $CaO–SiO_2–Al_2O_3$, in which δ–AlOOH is favored rather than forming a solid solution between $CaSiO_3$ and Al_2O_3. This observation also indicates that the Al^{3+} + $H^+ \rightarrow Si^{4+}$ substitution is not energetically favorable in the Ca-Pv system.

It is of interest to know the substitution mechanism of H in Ca-Pv. Because Ca-Pv is not quenchable, this question is challenging to address. From the Al-bearing glass experiments above, we can at least argue that Al^{3+} + $H^+ \rightarrow Si^{4+}$ would not play an important role for Ca-Pv. For dense pure SiO_2 polymorphs, $Si^{4+} \rightarrow 4H^+$ has been suggested (Spektor et al., 2011). In this case, the repulsion between 4H atoms in the octahedral site could increase the volume of the octahedra in the structure. In fact, it has been consistently observed that H_2O incorporation increases the unit-cell volume of SiO_2 (Spektor et al., 2011, 2016; Nisr et al., 2017b,a).

We measured the XRD patterns of Ca-Pv (Al free) synthesized from suolunite starting material in a Ne medium at 300 K during decompression. In this measurement, we measured diffraction patterns from multiples of spots in the sample, including the center of heating spots, the edge of heating spots, and in between. The dataset also contains diffraction patterns from spots obtained from high temperature heating runs to low temperature heating runs. Because the space group of Ca-Pv is controversial (Stixrude et al., 1996; Shim et al., 2002; Caracas et al., 2005; Jung and Oganov, 2005) and it is possible that H_2O incorporation can alter the crystal structure, we tentatively fit the patterns to the tetragonal *P4/mmm* cell (Shim et al., 2002). We plot the unit-cell volume data together with the compressional curve of anhydrous Ca-Pv from Chen et al. (2018) in Fig. 4. We found unusually high data scatter in the volume dataset. Most of the unit-cell volumes are systematically smaller than those of the anhydrous Ca-Pv throughout the pressure range we measured.

Some degree of the data scatter can originate from the deviatoric stress (Shim et al., 2000a). However, our experimental setup including a Ne medium is almost identical to the quasi-hydrostatic measurements of Chen et al. (2018). Such high data scatter was not observed in Chen

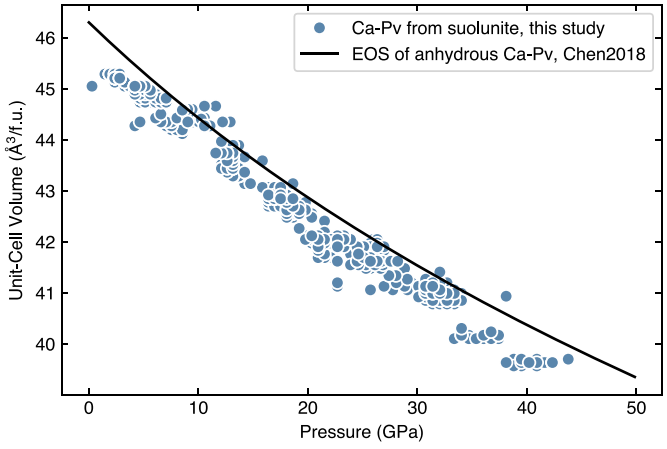

Fig. 4. The unit-cell volumes of Ca-Pv synthesized from H_2O-bearing starting material, suolunite at high pressure. For comparison, we plot the compressional curve of anhydrous Ca-Pv reported by Chen et al. (2018).

et al. (2018). The systematically smaller volume together with high-temperature peak splitting may indicate the incorporation of H_2O in the crystal structure of Ca-Pv. If so, it is feasible that the unit-cell volume of Ca-Pv changes with degree of hydration. The degree of hydration in NAMs could decrease with temperature (Demouchy et al., 2005). Given the fact that we measured unit-cell volumes from spots with heating to different temperatures, the data scatter could originate from different degree of hydration in Ca-Pv by temperature differences. While there are some data points slightly above the compressibility curve of anhydrous Ca-Pv in the dataset (Fig. 4), it is possible that those data points are contaminated with locally existing deviatoric stresses. Even if we take the amount of the offset of those larger volume data points as uncertainty, the shifts of the majority of data points can be regarded as significant.

If the dataset we presented in Fig. 4 indicates that H_2O incorporation can decrease the unit-cell volume of Ca-Pv, the substitution mechanism proposed for hydrous stishovite ($Si^{4+} \rightarrow 4H^{+}$) is unlikely. The reason is the direct substitution suggested results in an increase in the unit-cell volume of stishovite (Spektor et al., 2011; Nisr et al., 2017b,a) rather than decrease which is observed in our dataset for Ca-Pv. Also, stability of the tetragonal distortion at high temperatures could mean that hydrous Ca-Pv may have a larger magnitude of the structural deviation from the ideal cubic perovskite structure. Considering that silicate perovskite distortion is from the rigid body tilting of the SiO_6 octahedra (Woodward, 1997; Chen et al., 2018), and such rigid body tilting could be induced by mismatch of the larger cations in the A site (Ca for $CaSiO_3$ perovskite), it is possible that Ca defects might play an important role for the case of Ca-Pv. Such defects will have large impact for the unit-cell volume because of the size of Ca^{2+} ion and therefore will decrease the unit-cell volume substantially. In a natural $CaTiO_3$ perovskite sample, an IR study showed OH modes at 3320–3390 cm^{-1} at 1 bar (Beran et al., 1996). The reported IR mode frequency is very similar to that of the OH band we found for $CaSiO_3$ perovskite at 0.65 GPa (Fig. 2). Beran et al. (1996) interpreted that the IR signatures of $CaTiO_3$ perovskite is consistent with Ca vacancies.

Yet, in order to understand the substitution mechanism involving H, it is important to conduct more spectroscopy measurements. It would be also very useful to conduct density functional theory calculation to understand the substitution mechanism and energetics of different possible substitution mechanism in Ca-Pv involving H. Such attempts should be able to explain some key observations we made in this study: (1) the high-temperature stability of tetragonal distortion in hydrous Ca-Pv; (2) the frequency of the observed OH vibration from hydrous Ca-Pv and its high-pressure behavior; (3) the phase separation found in Al-bearing system (i.e., formation of δ-AlOOH from $CaSiO_3{\cdot}Al_2O_3$); and (4) the reduction in the unit-cell volume of Ca-Pv by hydration.

4. Implications

For the bulk lower mantle, the two major mineral phases, bridgmanite and ferropericlase, appear to have very limited storage capacity for H_2O at less than 200 ppm water (Panero et al., 2015; Bolfan-Casanova et al., 2002, 2003). We observed that the crystal structure and properties of Ca-Pv are severely affected by presence of H_2O in the starting materials. Furthermore, IR may support the incorporation of OH in Ca-Pv. The unit-cell volume behavior and the distortion indicate that the amount of H_2O in Ca-Pv could be much larger than a few tens to hundreds of ppm. Our IR estimation shows that the content could be up to 0.5–1 wt. % H_2O. If such an estimate is correct, Ca-Pv could be so far the most H_2O rich mineral among the NAMs in the lower mantle. We can also infer from our experiment that Ca-Pv would be an important H_2O storage candidate for Earth-like exoplanets with sufficient sizes. In fact, some stars have elevated Ca/Mg ratios, which can raise the amount of Ca-Pv in the Earth-like planets around those stars (Hinkel and Unterborn, 2018). The amount of Ca-Pv expected for the subducting mid-oceanic ridge basalt (MORB) is much higher (35 wt. %) (Hirose et al., 2005). Therefore, if the H_2O storage capacity of Ca-Pv is high, as suggested by our experimental observations, Ca-Pv in MORB could be the major source for deep water circulation.

We found that the partitioning behavior of Al is sensitive to the presence of H_2O in the system for $CaO–Al_2O_3–SiO_2$. We showed that Al comes out of the $CaSiO_3{\cdot}Al_2O_3$ starting material and form δ-AlOOH when H_2O is present in the system. Similar behavior was also documented for bridgmanite with H_2O where Al-bearing phase H was observed (Ohira et al., 2014). Therefore, these results demonstrate a significant change in the partitioning of Al in the lower mantle when H_2O exists as a chemical component in the system.

5. Conclusion

We showed experimentally that the crystal structure and some properties of Ca-Pv are different in H_2O bearing systems, $CaO–SiO_2–H_2O$ and $CaO–SiO_2–Al_2O_3–H_2O$. Tetragonal Ca-Pv structure remains stable at high temperatures unlike the case of anhydrous Ca-Pv. The unit-cell volume of Ca-Pv synthesized from hydrous starting materials is systematically smaller than anhydrous Ca-Pv and appears to be sensitive to degree of hydration. While challenging, our IR suggests that OH exists in the crystal structure of Ca-Pv and the amount can be 0.5–1.0 wt. %. In $CaO–SiO_2–Al_2O_3–H_2O$, Al forms a separate hydrous phase, δ-AlOOH, instead of remaining in Ca-Pv. For that experiment, Ca-Pv still showed the stability of tetragonal perovskite structure at high temperature, suggesting possible hydration of Ca-Pv. For more conclusive evidence for H_2O in Ca-Pv, it is desirable to develop reliable H_2O probe capable of measurements at in-situ high pressure, because of the instability of Ca-Pv at 1 bar. Density functional theory studies could be particularly useful for understanding possible H substitution mechanisms for Ca-Pv and our data would provide some useful properties to cross examine the results. It is also intriguing that the tetragonal Ca-Pv can be stabilized over cubic Ca-Pv in the hydrous lower mantle regions. If the tetragonal distortion develops sufficient anisotropy, it could be a useful property to seismologically investigate possible hydrated regions in the lower mantle.

CRediT authorship contribution statement

H. Chen: Data curation, Validation, Formal analysis, Investigation, Writing - original draft. **K. Leinenweber:** Conceptualization, Investigation, Resources, Writing - original draft, Funding acquisition. **V. Prakapenka:** Methodology. **C. Prescher:** Methodology. **Y. Meng:** Methodology. **H. Bechtel:** Methodology. **M. Kunz:** Methodology. **S.-H. Shim:** Conceptualization, Software, Formal analysis, Investigation, Resources, Writing - original draft, Visualization, Supervision, Funding acquisition.

Acknowledgments

We thank an anonymous reviewer and the editor for the comments and suggestions. The work has been supported by the NSF (EAR-1338810 and EAR-1725094) and NASA (80NSSC18K0353). H. C. and S.-H.S. were supported by a Keck grant (PI: P. Buseck). The results reported herein benefit from collaborations and information exchange within NASA's Nexus for Exoplanet System Science (NExSS) research coordination network sponsored by NASA's Science Mission Directorate. The synchrotron experiments were conducted at GSECARS (University of Chicago, Sector 13) and HPCAT (Sector 16), Advanced Photon Source (APS). GSECARS is supported by the NSF-Earth Science (EAR-1128799) and DOE-GeoScience (DE-FG02-94ER14466). HPCAT is supported by DOE-NNSA (DE-NA0001974) and DOE-BES (DE-FG02-99ER45775). APS is supported by DOE-BES under contract DE-AC02-06CH11357. This research used resources of the Advanced Light Source, which is a DOE Office of Science User Facility under contract no. DE-AC02-05CH11231. We acknowledge the use of facilities within

the Eyring Materials Center at Arizona State University. The experimental data for this paper are available by contacting SHDShim@asu.edu.

References

Akahama, Y., Kawamura, H., 2006. Pressure calibration of diamond anvil Raman gauge to 310 GPa. J. Appl. Phys. 100, 043516.

Beran, A., Libowitzky, E., Armbruster, T., 1996. A single-crystal infrared spectroscopic and x-ray-diffraction study of untwinned San Benito perovskite containing OH groups. Can. Mineral. 34, 803–809.

Bläß, U., Langenhorst, F., Frost, D., Seifert, F., 2007. Oxygen deficient perovskites in the system $CaSiO_3$-$CaAlO_{2.5}$ and implications for the Earth's interior. Phys. Chem. Miner. 34, 363–376.

Bolfan-Casanova, N., 2005. Water in the Earth's mantle. Mineral. Mag. 69, 229–257.

Bolfan-Casanova, N., Keppler, H., Rubie, D.C., 2000. Water partitioning between nominally anhydrous minerals in the MgO-SiO_2-H_2O system up to 24 GPa: implications for the distribution of water in the Earth's mantle. Earth Planet. Sci. Lett. 182, 209–221.

Bolfan-Casanova, N., Mackwell, S., Keppler, H., McCammon, C., Rubie, D., 2002. Pressure dependence of H solubility in magnesiowüstite up to 25 GPa: implications for the storage of water in the Earth's lower mantle. Geophys. Res. Lett. 29.

Bolfan-Casanova, N., Keppler, H., Rubie, D.C., 2003. Water partitioning at 660 km depth and evidence for very low water solubility in magnesium silicate perovskite. Geophys. Res. Lett. 30.

Caracas, R., Wentzcovitch, R., Price, G.D., Brodholt, J., 2005. $CaSiO_3$ perovskite at lower mantle pressures. Geophys. Res. Lett. 32, L06306.

Chen, H., Shim, S.H., Leinenweber, K., Prakapenka, V., Meng, Y., Prescher, C., 2018. Crystal structure of $CaSiO_3$ perovskite at 28–62 GPa and 300 K under quasi-hydrostatic stress conditions. Am. Mineral.: J. Earth Planet. Mater. 103, 462–468.

Demouchy, S., Deloule, E., Frost, D.J., Keppler, H., 2005. Pressure and temperature-dependence of water solubility in Fe-free wadsleyite. Am. Mineral. 90, 1084–1091.

Duan, Y., Sun, N., Wang, S., Li, X., Guo, X., Ni, H., Prakapenka, V.B., Mao, Z., 2018. Phase stability and thermal equation of state of δ-AlOOH: implication for water transportation to the deep lower mantle. Earth Planet. Sci. Lett. 494, 92–98.

Eggleton, R., Ringwood, A., 1978. High pressure synthesis of a new aluminium silicate: $Al_5Si_5O_{17}(OH)$. Geochem. J. 12, 191–194.

Frost, D.J., Fei, Y., 1998. Stability of phase D at high pressure and high temperature. J. Geophys. Res. Solid Earth 103, 7463–7474.

Gleason, A., Quiroga, C., Suzuki, A., Pentcheva, R., Mao, W., 2013. Symmetrization driven spin transition in ε-FeOOH at high pressure. Earth Planet. Sci. Lett. 379, 49–55.

Goncharov, A., Struzhkin, V., Somayazulu, M., Hemley, R., Mao, H., 1996. Compression of ice to 210 gigapascals: infrared evidence for a symmetric hydrogen-bonded phase. Science 273, 218–220.

Gréaux, S., Nishiyama, N., Kono, Y., Gautron, L., Ohfuji, H., Kunimoto, T., Menguy, N., Irifune, T., 2011. Phase transformations of $Ca_3Al_2Si_3O_{12}$ grossular garnet to the depths of the Earth's mantle transition zone. Phys. Earth Planet. Inter. 185, 89–99.

Hinkel, N.R., Unterborn, C.T., 2018. The star-planet connection. I. Using stellar composition to observationally constrain planetary mineralogy for the 10 closest stars. Astrophys. J. 853, 83.

Hirose, K., Takafuji, N., Sata, N., Ohishi, Y., 2005. Phase transition and density of subducted MORB crust in the lower mantle. Earth Planet. Sci. Lett. 237, 239–251.

Inoue, T., Yurimoto, H., Kudoh, Y., 1995. Hydrous modified spinel, $Mg_{1.75}SiH_{0.5}O_4$: a new water reservoir in the mantle transition region. Geophys. Res. Lett. 22, 117–120.

Jung, D.Y., Oganov, A.R., 2005. Ab initio study of the high-pressure behavior of $CaSiO_3$ perovskite. Phys. Chem. Miner. 32, 146–153.

Kesson, S., Gerald, J.F., Shelley, J., 1998. Mineralogy and dynamics of a pyrolite lower mantle. Nature 393, 252.

Kudoh, Y., Kuribayashi, T., Suzuki, A., Ohtani, E., Kamada, T., 2004. Space group and hydrogen sites of δ-AlOOH and implications for a hypothetical high-pressure form of $Mg(OH)_2$. Phys. Chem. Miner. 31, 360–364.

Kurashina, T., Hirose, K., Ono, S., Sata, N., Ohishi, Y., 2004. Phase transition in Al-bearing $CaSiO_3$ perovskite: implications for seismic discontinuities in the lower mantle. Phys. Earth Planet. Inter. 145, 67–74.

Lin, J.F., Militzer, B., Struzhkin, V.V., Gregoryanz, E., Hemley, R.J., Mao, H.k., 2004. High pressure-temperature raman measurements of H_2O melting to 22 GPa and 900 K. J. Chem. Phys. 121, 8423–8427.

Litasov, K., Ohtani, E., Langenhorst, F., Yurimoto, H., Kubo, T., Kondo, T., 2003. Water solubility in Mg-perovskites and water storage capacity in the lower mantle. Earth Planet. Sci. Lett. 211, 189–203.

Litasov, K.D., Kagi, H., Shatskiy, A., Ohtani, E., Lakshtanov, D.L., Bass, J.D., Ito, E., 2007. High hydrogen solubility in Al-rich stishovite and water transport in the lower mantle. Earth Planet. Sci. Lett. 262, 620–634.

Liu, J., Hu, Q., Kim, D.Y., Wu, Z., Wang, W., Xiao, Y., Chow, P., Meng, Y., Prakapenka, V.B., Mao, H.K., et al., 2017. Hydrogen-bearing iron peroxide and the origin of ultralow-velocity zones. Nature 551, 494.

Ma, Z., Shi, N., Mou, G., Liao, L., 1999. Crystal structure refinement of suolunite and its significance to the cement techniques. Chin. Sci. Bull. 44, 2125–2130.

Mao, H., Bell, P., Shaner, J.t., Steinberg, D., 1978. Specific volume measurements of Cu, Mo, Pd, and Ag and calibration of the ruby R1 fluorescence pressure gauge from 0.06 to 1 Mbar. J. Appl. Phys. 49, 3276–3283.

Meng, Y., Shen, G., Mao, H.K., 2006. Double-sided laser heating system at HPCAT for in situ x-ray diffraction at high pressures and high temperatures. J. Phys. Condens. Matter 18, S1097–103.

Murakami, M., Hirose, K., Yurimoto, H., Nakashima, S., Takafuji, N., 2002. Water in Earth's lower mantle. Science 295, 1885–1887.

Navrotsky, A., 1999. A lesson from ceramics. Science 284, 1788–1789.

Németh, P., Leinenweber, K., Ohfuji, H., Groy, T., Domanik, K.J., Kovács, I.J., Kovács, J.S., Buseck, P.R., 2017. Water-bearing, high-pressure Ca-silicates. Earth Planet. Sci. Lett. 469, 148–155.

Newville, M., Stensitzki, T., Allen, D., Ingargiola, A., 2015. Non-linear least-squares minimization and curve-fitting for python. Chicago, IL.

Nishi, M., Irifune, T., Tsuchiya, J., Tange, Y., Nishihara, Y., Fujino, K., Higo, Y., 2014. Stability of hydrous silicate at high pressures and water transport to the deep lower mantle. Nat. Geosci. 7, 224–227.

Nishi, M., Kuwayama, Y., Tsuchiya, J., Tsuchiya, T., 2017. The pyrite-type high-pressure form of FeOOH. Nature 547, 205.

Nisr, C., Shim, S.H., Leinenweber, K., Chizmeshya, A., 2017b. Raman spectroscopy of water-rich stishovite and dense high-pressure silica up to 55 GPa. Am. Mineral. 102, 2180–2189.

Nisr, C., Leinenweber, K., Prakapenka, V., Prescher, C., Tkachev, S., Dan Shim, S.H., 2017a. Phase transition and equation of state of dense hydrous silica up to 63 GPa. J. Geophys. Res. Solid Earth.

Ohira, I., Ohtani, E., Sakai, T., Miyahara, M., Hirao, N., Ohishi, Y., Nishijima, M., 2014. Stability of a hydrous δ-phase, AlOOH-$MgSiO_2(OH)_2$, and a mechanism for water transport into the base of lower mantle. Earth Planet. Sci. Lett. 401, 12–17.

Ohtani, E., 2015. Hydrous minerals and the storage of water in the deep mantle. Chem. Geol. 418, 6–15.

Panero, W.R., Pigott, J.S., Reaman, D.M., Kabbes, J.E., Liu, Z., 2015. Dry $(Mg,Fe)SiO_3$ perovskite in the Earth's lower mantle. J. Geophys. Res. Solid Earth 120, 894–908.

Paterson, M., 1982. The determination of hydroxyl by infrared absorption in quartz, silicate glasses and similar materials. Bull. Mineral. 105, 20–29.

Pawley, A.R., McMillan, P.F., Holloway, J.R., 1993. Hydrogen in stishovite, with implications for mantle water content. Science 261 1024–1024.

Prakapenka, V.B., Kubo, A., Kuznetsov, A., Laskin, A., Shkurikhin, O., Dera, P., Rivers, M.L., Sutton, S.R., 2008. Advanced flat top laser heating system for high pressure research at GSECARS: application to the melting behavior of germanium. High Press. Res. 28, 225–235.

Prescher, C., Prakapenka, V.B., 2015. DIOPTAS: a program for reduction of two-dimensional X-ray diffraction data and data exploration. High Press. Res. 35, 223–230.

Rivers, M., Prakapenka, V.B., Kubo, A., Pullins, C., Holl, C.M., Jacobsen, S.D., 2008. The COMPRES/GSECARS gas-loading system for diamond anvil cells at the Advanced Photon Source. High Press. Res. 28, 273–292.

Sano, A., Ohtani, E., Kondo, T., Hirao, N., Sakai, T., Sata, N., Ohishi, Y., Kikegawa, T., 2008. Aluminous hydrous mineral δ-AlOOH as a carrier of hydrogen into the core-mantle boundary. Geophys. Res. Lett. 35.

Schwegler, E., Sharma, M., Gygi, F., Galli, G., 2008. Melting of ice under pressure. Proc. Natl. Acad. Sci. 105, 14779–14783.

Shaw, S., Clark, S., Henderson, C., 2000. Hydrothermal formation of the calcium silicate hydrates, tobermorite $(Ca_5Si_6O_{16}(OH)_2{\cdot}4H_2O)$ and xonotlite $(Ca_6Si_6O_{17}(OH)_2)$: an in situ synchrotron study. Chem. Geol. 167, 129–140.

Shim, S.H., 2017. PeakPo - A python software for X-ray diffraction analysis at high pressure and high temperature. https://doi.org/10.5281/zenodo.810200.

Shim, S.-H., Duffy, T.S., Shen, G., 2000a. The equation of state of $CaSiO_3$ perovskite to 108 GPa at 300 K. Phys. Earth Planet. Inter. 120, 327–338.

Shim, S.H., Duffy, T.S., Shen, G., 2000b. The stability and P–V–T equation of state of $CaSiO_3$ perovskite in the Earth's lower mantle. J. Geophys. Res. Solid Earth 105, 25955–25968.

Shim, S.H., Jeanloz, R., Duffy, T.S., 2002. Tetragonal structure of $CaSiO_3$ perovskite above 20 GPa. Geophys. Res. Lett. 29, 2166.

Smyth, J., Frost, D., Nestola, F., Holl, C., Bromiley, G., 2006. Olivine hydration in the deep upper mantle: effects of temperature and silica activity. Geophys. Res. Lett. 33.

Spektor, K., Nylen, J., Stoyanov, E., Navrotsky, A., Hervig, R.L., Leinenweber, K., Holland, G.P., Häussermann, U., 2011. Ultrahydrous stishovite from high-pressure hydrothermal treatment of SiO_2. Proc. Natl. Acad. Sci. 108, 20918–20922.

Spektor, K., Nylen, J., Mathew, R., Edén, M., Stoyanov, E., Navrotsky, A., Leinenweber, K., Häussermann, U., 2016. Formation of hydrous stishovite from coesite in high-pressure hydrothermal environments. Am. Mineral. 101, 2514–2524.

Stixrude, L., Cohen, R.E., Yu, R., Krakauer, H., 1996. Prediction of phase transition in $CaSiO_3$ perovskite and implications for lower mantle structure.

Suzuki, A., Ohtani, E., Kamada, T., 2000. A new hydrous phase δ-AlOOH synthesized at 21 GPa and 1000 °C. Phys. Chem. Miner. 27, 689–693.

Tangeman, J.A., Phillips, B.L., Navrotsky, A., Weber, J.K.R., Hixson, A.D., Key, T.S., 2001. Vitreous forsterite (Mg_2SiO_4): synthesis, structure, and thermochemistry. Geophys. Res. Lett. 28, 2517–2520.

Wang, Y., Weidner, D.J., Guyot, F., 1996. Thermal equation of state of $CaSiO_3$ perovskite. J. Geophys. Res. 101, 661–672.

Wolanin, E., Pruzan, P., Chervin, J., Canny, B., Gauthier, M., Häusermann, D., Hanfland, M., 1997. Equation of state of ice VII up to 106 GPa. Phys. Rev. B 56, 5781.

Woodward, P.M., 1997. Octahedral tilting in perovskites. I. Geometrical considerations. Acta Crystallogr. Sect. B: Struct. Sci. 53, 32–43.

Ye, Y., Prakapenka, V., Meng, Y., Shim, S.H., 2017. Intercomparison of the gold, platinum, and Mgo pressure scales up to 140 GPa and 2500 K. J. Geophys. Res. Solid Earth 122, 3450–3464.

Ye, Y., Smyth, J.R., Hushur, A., Manghnani, M.H., Lonappan, D., Dera, P., Frost, D.J., 2010. Crystal structure of hydrous wadsleyite with 2.8% H_2O and compressibility to 60 GPa. Am. Mineral. 95, 1765–1772.